As originally published in the IPC APEX EXPO Conference Proceedings.

Thermal Cycling Reliability Screening of Multiple Pb-free Solder Ball Alloys

Joe Smetana[1], Richard Coyle[1], and Peter Read[1]
Thomas Koshmeider[2], Dave Love[3],
Mark Kolenik[4], and Jennifer Nguyen[5]
[1]Alcatel-Lucent, [2]Freescale Semiconductor, [3]Sun Microsystems, [4] Philips Medical, [5]Flextronics

ABSTRACT
Thermal cycling tests were conducted using two different ceramic ball grid array (CBGA) test vehicles having balls comprised of nine different Pb free solder alloys. The experiment was designed as a screening experiment to obtain data comparing thermal fatigue reliability of the various solder ball alloys. The test matrix was dominated by commercial SnAgCu (SAC) alloys but also included other high, low, and no-Ag alloys. The surface mount assembly was done with SAC305 (Sn3Ag0.5Cu) solder paste. The thermal cycling data, Weibull analyses, and metallographic failure analysis indicate that the best thermal fatigue performance was obtained with higher Ag alloys.

INTRODUCTION
Solder suppliers have introduced a significant number of new Pb-free BGA solder ball alloys whose compositions deviate from the mainstream SAC alloys that contain 3-4% silver and 0.5 to 0.8% copper. Most of these alloys have been introduced to address susceptibility to drop and shock failure. In general, these alloys have lower silver (Ag) content because lowering the Ag content is believed to enhance resistance to failure during high strain rate loading conditions [1-12]. However, very little data is available on the thermal fatigue performance of these alloys and much of the published data was released after the start of this test program [1-5]. Thermal fatigue performance is very important to many in the high reliability user community where the drop/shock performance associated with hand-held consumer products is not critical. The limited data available suggests that thermal fatigue performance may be significantly different between the various alloys. However, many of the components used in high volume, lower product life, hand-held consumer products ultimately are deployed in high-reliability products. Without thermal fatigue data, it is very difficult to make intelligent decisions on the viability of components using any of the alternate Pb-free alloys.

EXPERIMENTAL
Test Strategy
The experimental program was designed as a rapid, limited sample size thermal cycling test to screen and compare the thermal fatigue performance of multiple Pb free solder alloys. The printed board and component test vehicles were developed in a previous program, which enabled quick execution at the front end of the test program as well as providing some baseline performance data.

Alloy Selection
The Pb-free alloys evaluated in this program and their nominal compositions are listed in Table 1. Because there is considerable experience throughout the industry with the high Ag content, SAC405 alloy, that alloy is considered the control alloy in the experimental group. The alloys are grouped in the table by Ag content, with high, low, and near-zero or zero per cent Ag.

Table 1. Nominal compositions of the Pb free alloys evaluated in the test program.

Alloy Designation	Ag wt%	Cu wt%	Other wt%	Sn wt%
SAC405	4.0	0.5		Balance
Sn3.5Ag	3.5	0		
SAC310	3.0	1.0		
SAC205N*	2.0	0.5	Ni 0.05	
LF35	1.2	0.5	Ni 0.005	
SAC108	1.0	0.8		
SAC105	1.0	0.5		
SACX**	0.3	0.7	Ni 0.025	
SN100C	0	0.5-0.7	Ni 0.1	
* SAC205 +Ni ** SAC0307 plus dopants (Cookson proprietary alloy)				

Component and Board Test Vehicle Descriptions

The component used for this testing is based on Freescale Semiconductor ceramic ball grid array (CBGA) daisy chain test component. The ceramic substrate measures 27 mm x 27 mm and is purchased as a land grid array (LGA). Balls are attached afterwards to create either a full or a perimeter array BGA. The full array has 483 I/O with one corner ball depopulated and the depopulated or perimeter array has only the outer 3 rows populated, with the center of the array left depopulated. Figure 1 shows a photograph of the full and depopulated component arrays in the “dead bug” position.

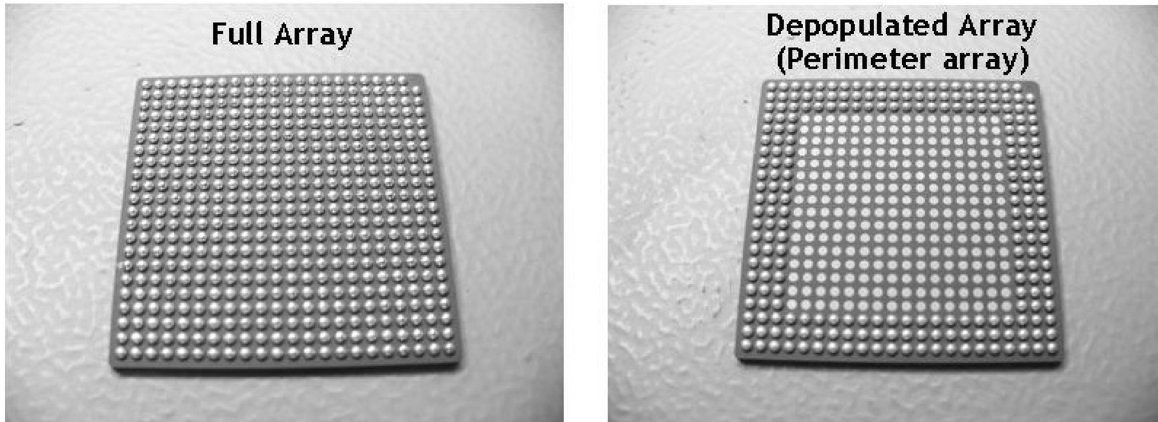

Figure 1. The CBGA component shown with fully populated array (left) and depopulated or perimeter array (right).

The schematic of the test board is shown in Figure 2. It is a 6 layer board with dimensions of 4.5 x 8.9 x 0.093 inches and has individual islands for each of the 8 component locations to facilitate component removal. The gold finger edge connector at one end of this board is specifically designed to mate with the event detector cable used for resistance monitoring during thermal cycle testing. The material used in PCB fabrication was Isola 370HR, a filled phenolic Pb-free compatible FR4. The board finish is immersion silver.

A key benefit of this component/board test vehicle combination is that it was used previously with high Ag Pb free alloys and was shown to produce failures rapidly, in the order of 1000 cycles. For the temperature cycle used in this experiment, this fulfilled the requirement for a relatively short elapsed test time of less than 3 months. An additional benefit is provided by the large diameter of the solder balls (0.89mm), which minimizes the effect the assembly solder paste SAC305 alloy has on the final alloy composition of the assembled solder joints.

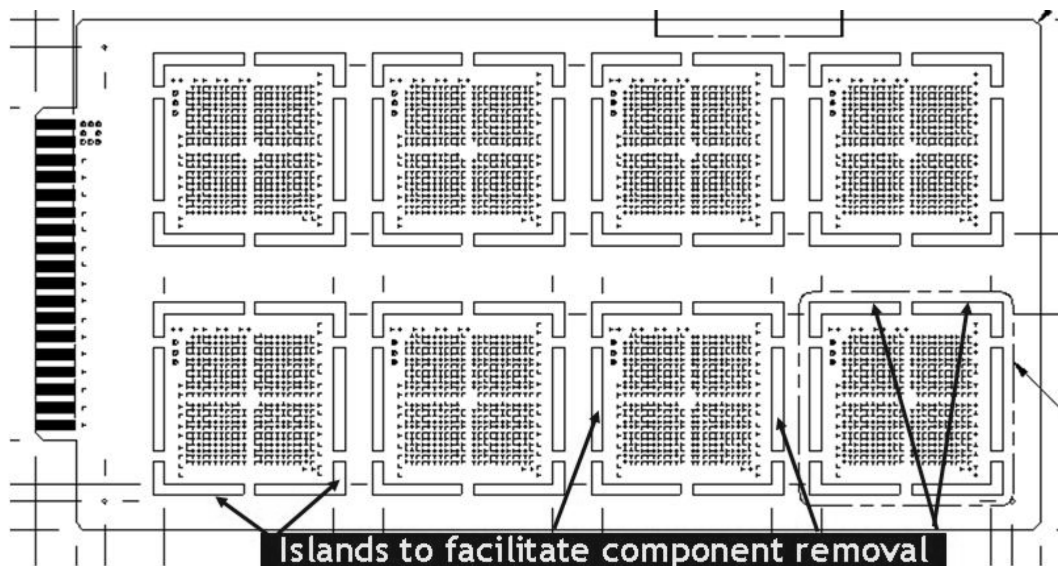

Figure 2. Schematic drawing of the 8-up daisy chained test board.

Sample Size

The sample sized used for each alloy was limited to keep the size of the test manageable while enabling testing of as many alloys as possible. A total of 16 each of the fully populated CBGAs, and 8 each of the depopulated CBGAs were tested per

alloy. On the full arrays, both the outer and inner array nets were monitored. Table 2 details the test matrix and board identification.

Table 2. The details of the Multiple Alloy test matrix and board identification.

Multiple Alloy Screening Project								
Alloy	Populated or Depopulated	Component Identification	# Components Required	# Bare Boards	Assembly Alloy	Comments	Board #	Board Identification
SAC405	Full	SAC405F	16	2	SAC305	Control	62-63	M_SAC405F
SAC405	Depopulated	SAC405D	8	1	SAC305	Control	64	M_SAC405D
SnAg (Sn3.5Ag)	Full	SnAgF	16	2	SAC305		68-69	M_SnAgF
SnAg (Sn3.5Ag)	Depopulated	SnAgD	8	1	SAC305		70	M_SnAgD
Sn100C	Full	Sn100CF	16	2	SAC305		74-75	M_Sn100CF
Sn100C	Depopulated	Sn100CD	8	1	SAC305		76	M_Sn100CD
Sn1.2Ag0.5Cu0.005Ni (LF35)	Full	LF35F	16	2	SAC305		77-78	M_LF35F
Sn1.2Ag0.5Cu0.005Ni (LF35)	Depopulated	LF35D	8	1	SAC305		79	M_LF35D
SAC205 + Nickel (.05% Ni)	Full	SAC205NF	16	2	SAC305		80-81	M_SAC205NF
SAC205 + Nickel (.05% Ni)	Depopulated	SAC205ND	8	1	SAC305		82	M_SAC205ND
SAC310 + 1% Cu	Full	SAC310F	16	2	SAC305		83-84	M_SAC310F
SAC310 + 1% Cu	Depopulated	SAC310D	8	1	SAC305		85	M_SAC310D
SAC105	Full	SAC105F	16	2	SAC305		86-87	M_SAC105F
SAC105	Depopulated	SAC105D	8	1	SAC305		88	M_SAC105D
SAC108	Full	SAC108F	16	2	SAC305		89-90	M_SAC108F
SAC108	Depopulated	SAC108D	8	1	SAC305		91	M_SAC108D
SACX	Full	SACXF	16	2	SAC305		92-93	M_SACXF
SACX	Depopulated	SACXD	8	1	SAC305		94	M_SACXD
		Totals	216	27				
Comments:	8 components per board							

Surface Mount Assembly Details

Surface mount assembly was typical of a Pb-free manufacturing assembly process. The equipment used for assembly is shown in Table 3. A 6 mil thick laser cut stencil with 27 mil round aperture openings was used for the build. The solder paste openings were designed to match the pad size on the bare board (see Figure 3). This results in a theoretical solder paste volume of 3435 cubic mils. The solder paste used was a type 3, no-clean solder paste with an alloy composition of 96.5Sn3Ag0.5Cu and a metal percentage of 89%. The actual solder paste volume as measured on the board is detailed in Figure 4. The estimated final composition of each alloy solder joint after assembly with SAC305 paste is shown in Table 4. These calculations are based on the solder volume shown in Figure 4 and are derived from the J. Pan calculator [18]. The calculations do not account for dissolution effects from either package or board pads or finishes. The Pb free reflow profile and thermocouple locations are identified in Figure 5. A photograph of the finished assembly is shown in Figure 6.

Table 3. Equipment used for the Pb free assembly of the Alloy Screening test vehicles.

Machine	Manufacturer/ Model
Printer	DEK265 Horizon
Pick and Place	Siemens Siplace
Reflow	Heller 1800EXL
Solder Paste Measurements	CyberOptics
X-ray	Dage

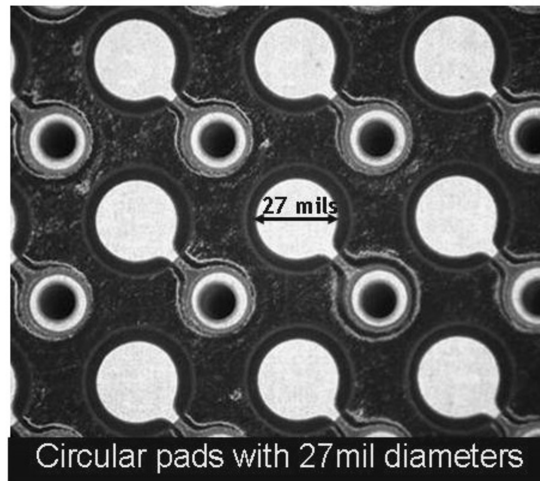

Figure 3. Typical circular CBGA assembly pad sites with 27 mil diameters.

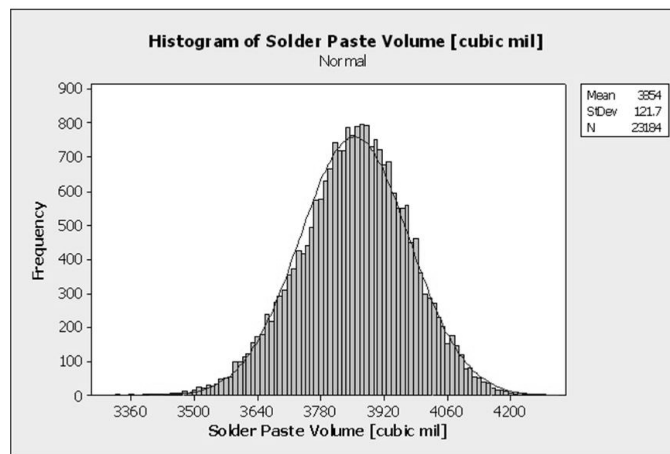

Figure 4. Histogram of measured solder paste volumes.

Table 4. Theoretical change in solder ball composition due to assembly with SAC305 solder paste.

Alloy Name	Ball Composition (Balance Sn) %			Theoretical Final Composition (Balance Sn) %	
	Ag	Cu	Other	Ag	Cu
SAC 405	4	0.5	NA	3.92	0.50
SnAg	3.5	0	NA	3.46	0.04
SN100C	0	0.7	.05Ni +Ge	0.24	0.68
LF35	1.2	0.5	.005 Ni	1.35	0.50
SAC205+N	2	0.5	.05 Ni	2.08	0.50
SAC310	3	1.0	NA	3.00	0.96
SAC105	1	0.5	NA	1.16	0.50
SAC108	1	0.8	NA	1.16	0.78
SACX0307	0.3	0.7	Bi + X	0.52	0.68

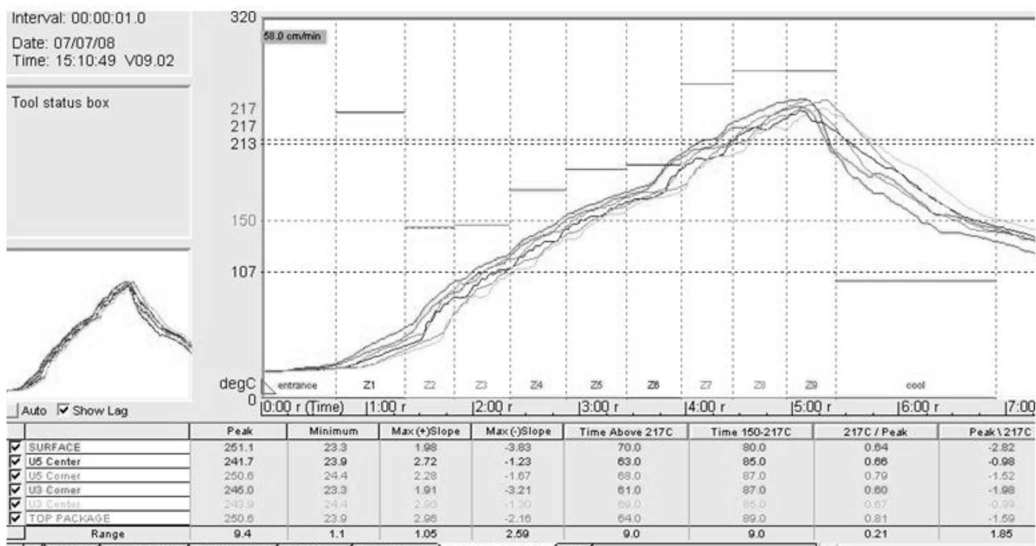

	Peak	Minimum	Max (+)Slope	Max (-)Slope	Time Above 217C	Time 150-217C	217C / Peak	Peak \ 217C
SURFACE	251.1	23.3	1.98	-3.83	70.0	80.0	0.64	-2.82
U5 Center	241.7	23.9	2.72	-1.23	63.0	85.0	0.66	-0.98
U5 Corner	250.6	24.4	2.28	-1.67	68.0	87.0	0.79	-1.52
U3 Corner	246.0	23.3	1.91	-3.21	61.0	87.0	0.60	-1.98
U3 Center	243.9	24.4	2.90	-1.30	69.0	85.0	0.67	-0.99
TOP PACKAGE	250.6	23.9	2.96	-2.16	64.0	89.0	0.81	-1.59
Range	9.4	1.1	1.05	2.59	9.0	9.0	0.21	1.85

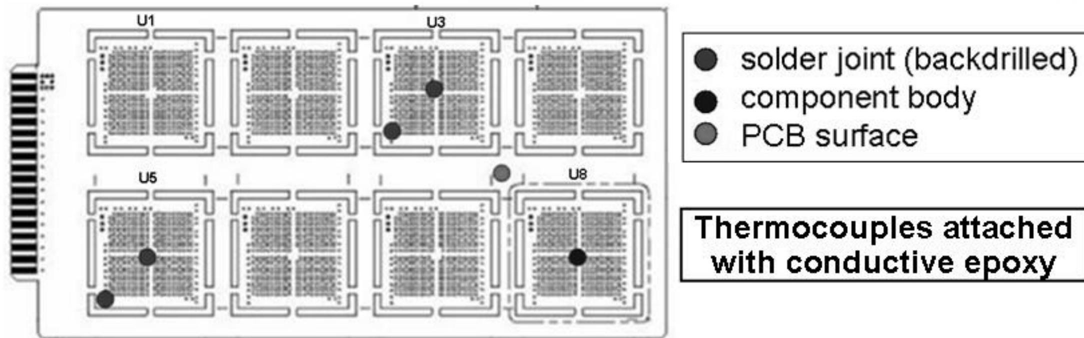

Figure 5. Pb free assembly reflow profile and thermocouple attachment locations.

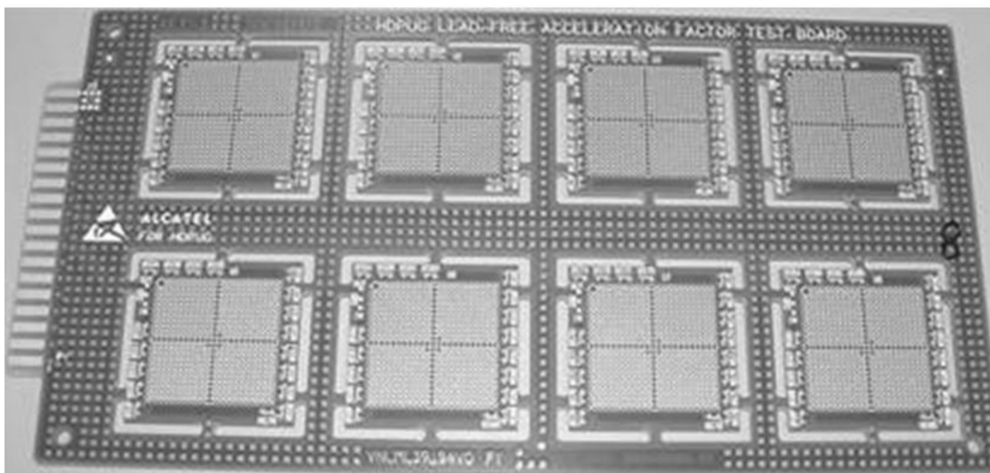

Figure 6. Photograph of finished PCB test vehicle assembly.

Post-Assembly Inspection

After assembly, all components were examined for solder process voiding using transmission x-ray. There was no major voiding detected and there were no differences seen between the different alloys. The components and the test circuit boards were daisy chained, which enabled electrical continuity testing after surface mount assembly. After assembly, all nets were tested successfully.

Thermal Cycling

The components and the test circuit boards were daisy chained to allow in situ, continuous monitoring during thermal cycling. The resistance of each loop was independently monitored during the temperature cycle testing. All assembled circuit boards

were thermally cycled from 0 °C to 100 °C with 10 minute ramps between temperature extremes and 30 minute dwells at each temperature extreme in accordance with the IPC-9701A industry test standard [19]. The solder joints were monitored continuously during thermal cycling with an event detector set at a resistance limit of 300 ohms or higher. The CBGA has a typical time zero resistance through the daisy chain net of about 15 Ohms. A spike of greater than 300 ohms for 0.2 microseconds followed by 9 additional events within 10% of the cycles to the initial event is flagged as a failure. The failure data are reported as characteristic life η (number of cycles to 63.2% failure) and slope β from a two-parameter Weibull analysis.

Weibull and Regression Analysis

Extensive Weibull and regression analysis was completed on the failure data. Figures 7 and 8 show the Weibull plots for the full arrays and figures 9 and 10 show the Weibull plots for the depopulated arrays respectively. For clarity these have been separated into high silver alloys (2% or greater Ag) and lower silver alloys (less than 2% silver). The data also are summarized in Table 5. See the appendix for individual Weibull plots by specific alloy. These individual plots also separate early from late failures. Inner row failures on the full arrays were also monitored, but are not shown here as they are of limited value and are clearly affected by the outer row failures. For the full arrays, there is an anomaly in the data in roughly the 700-900 cycle range where there are very few failures on any of the alloys. There were no chamber events to explain this anomaly and extensive failure analysis, detailed later, was done in an attempt to understand this data. Two separate failure modes were identified. As a result the Weibull beta values for the full arrays are in general lower than what would normally be expected. For the depopulated arrays, this anomaly is not seen and the Weibull beta values were much more as expected. The depopulated components failed considerably faster than the full arrays. However, failure analysis showed that many of these failures were also not typical fatigue failures.

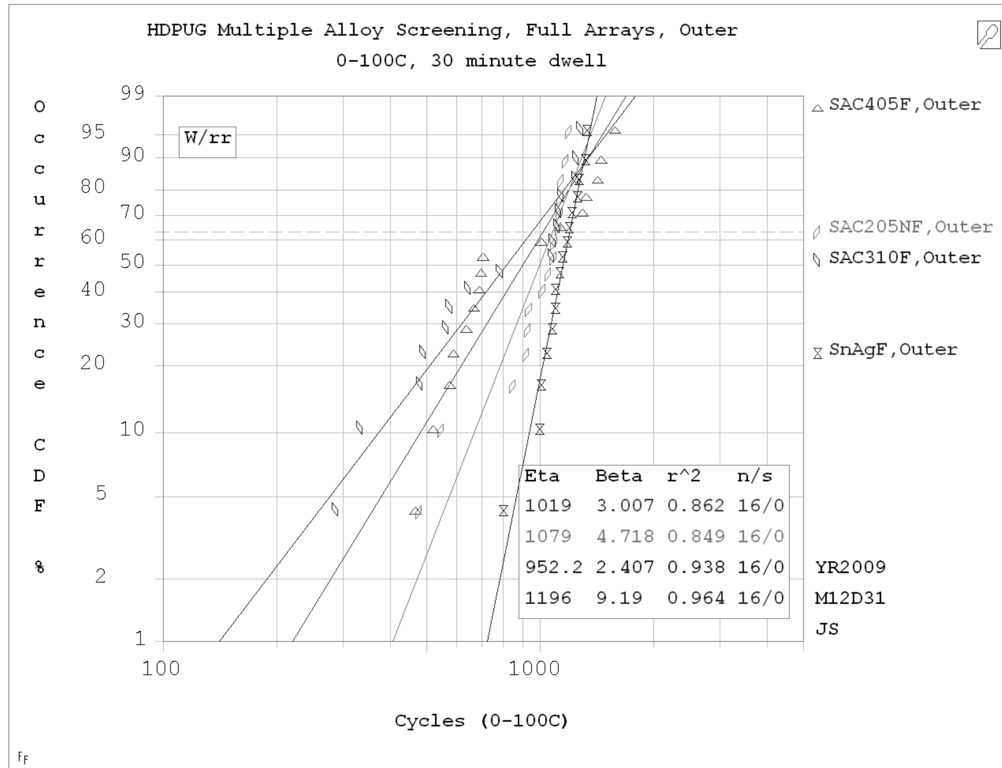

Figure 7. Weibull plot of the high silver alloy CBGA Full Arrays

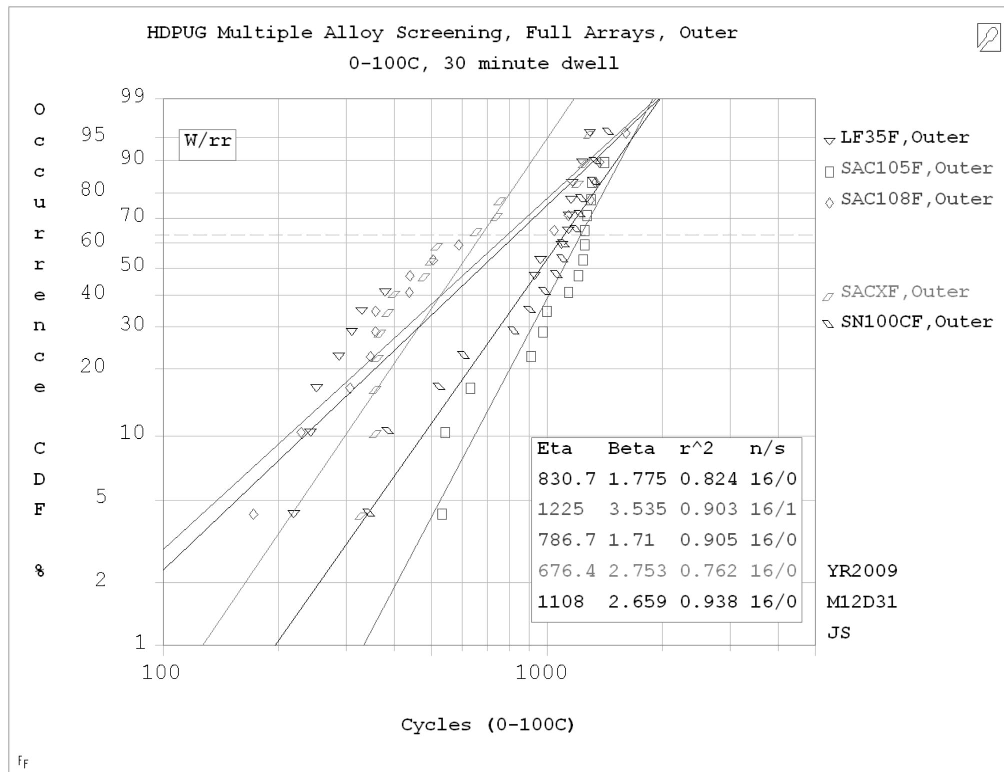

Figure 8. Weibull plot of the low silver alloy CBGA full arrays.

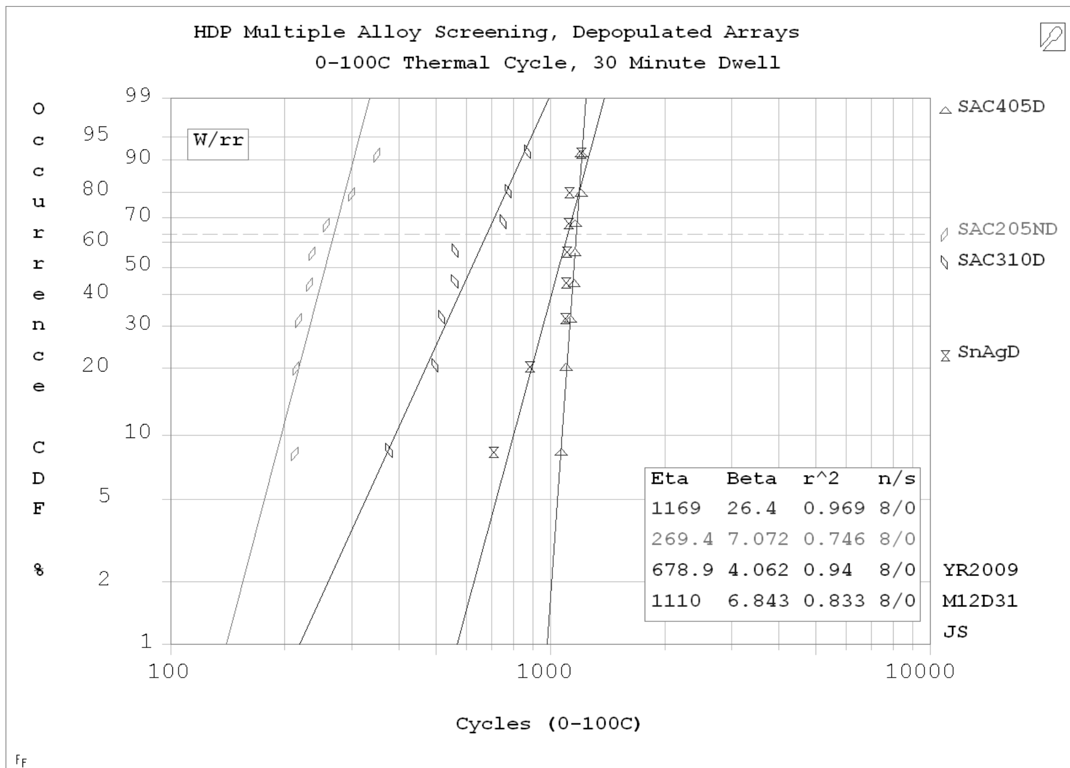

Figure 9. Weibull plot of the high silver alloy CBGA Depopulated Arrays

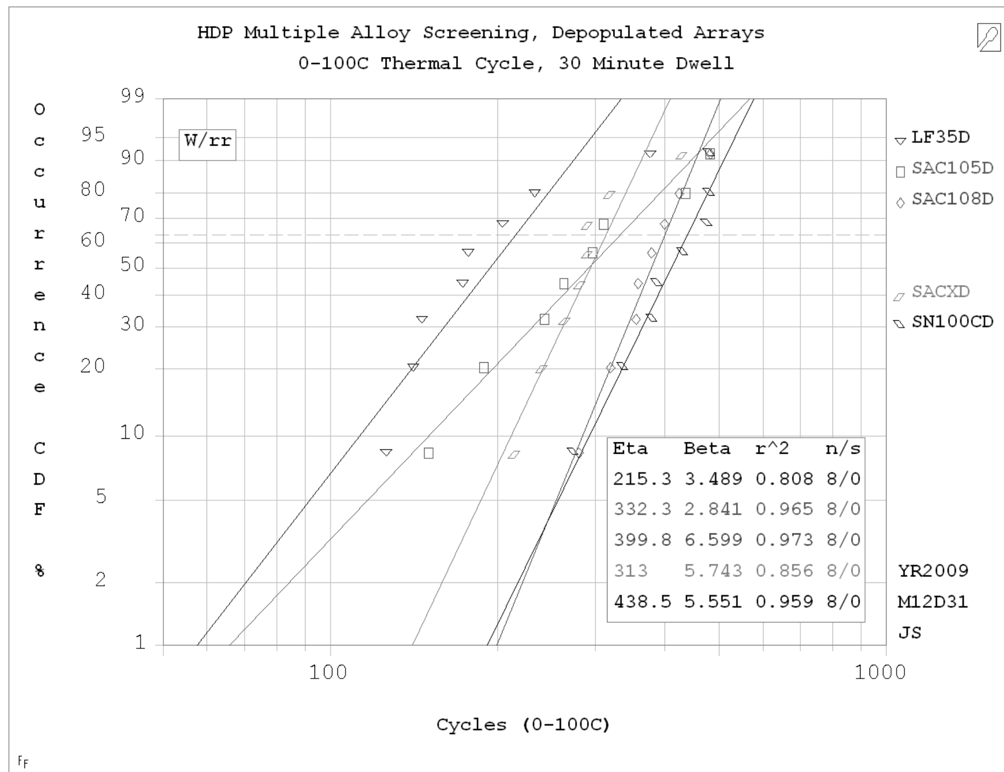

Figure 10. Weibull plot of the low silver alloy CBGA Depopulated Arrays.

Table 5. Summary of characteristic lifetimes (η)and slopes (β) for Pb free alloys tested in full and depopulated (perimeter) arrays

Pb free Alloy	Full Array		Depopulated (Perimeter) Array	
	η	β	η	β
SAC405	1019	3.0	1169	26.4
Sn3.5Ag	1196	9.2	1110	6.8
SAC310	952	2.4	678	4.1
SN100C	1108	2.7	439	5.6
SAC108	787	1.7	400	6.6
SAC105	1225	3.5	332	2.8
SACX	676	2.8	313	5.7
SAC205N	1079	4.7	269	7.1
LF35	831	1.8	215	3.5

.

Because of the anomaly noted previously, each alloy was plotted separating the “early group” of failures (before roughly the 700-900 cycle range) and the “late group” into separate analysis. The combined analysis was also done. This is detailed in Appendix A.

Figures 11 and 12 show the rankings of the full and depopulated arrays. For the full arrays, the ranking shown here is based only on the failures from the early group of failures. In all cases the blue bars represent eta (characteristic life) and the burgundy bars represent the 1% failure rate based on the Weibull data.

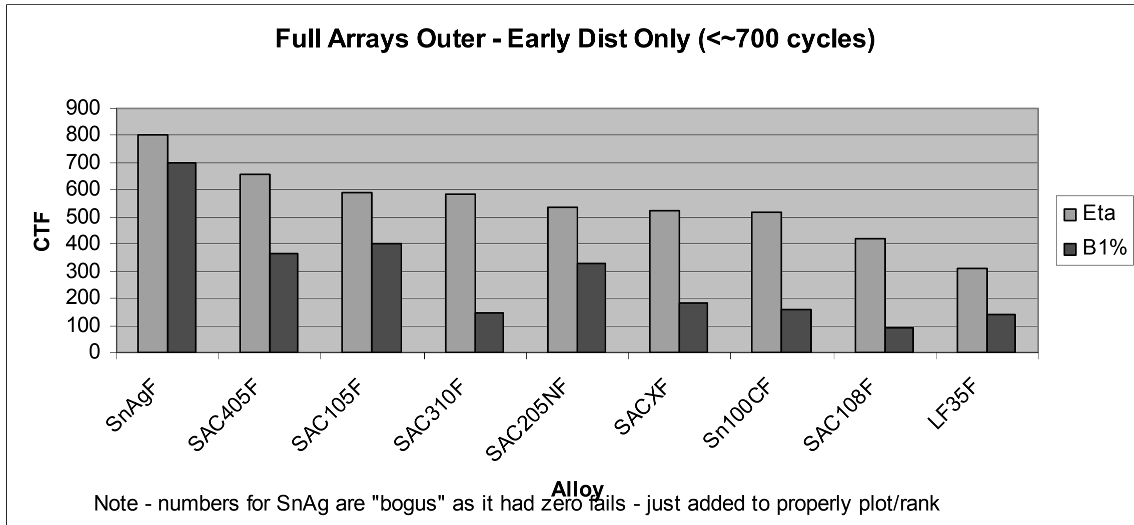

Figure 11: Ranking of the performance of the full arrays by alloy. This data includes only the failures before approximately 700 cycles.

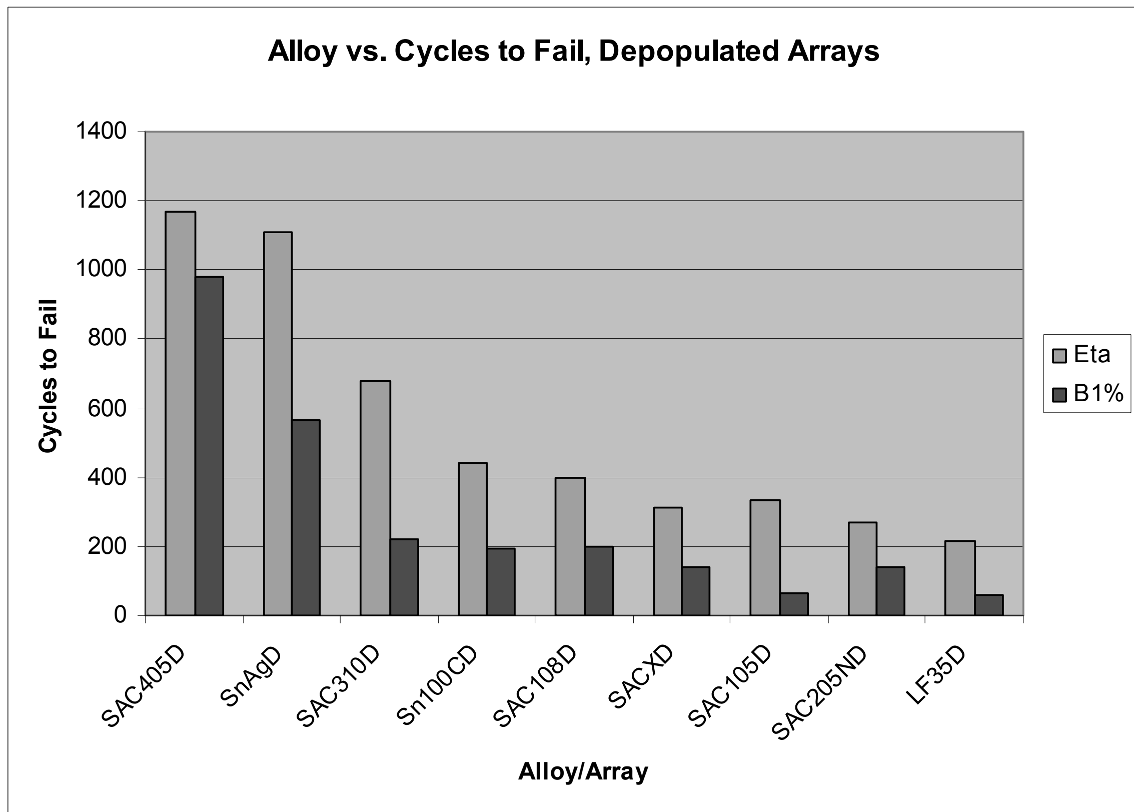

Figure 12. Ranking of the Weibull performance of the Depopulated Arrays

FAILURE ANALYSIS

Methodology

Several anomalies in the experimental data were discussed in the previous section entitled **Weibull and Regression Analysis**. The data from the Weibull plots presented previously in Figures 7 and 8 are summarized again in a modified version of Table 5. The shaded areas indicate test cells selected for metallographic failure analysis. Viewing the data in tabular format facilitates anomaly recognition and the test cell comparisons. Anomalous behavior includes: 1) the performance of some alloys differs significantly between full and depopulated arrays, 2) many of the test cells are characterized by atypically low Weibull slopes (β<3.0), and 3) some lower Ag alloys appear to outperform the higher Ag alloys. This third anomaly

contradicts published reports that Ag content controls thermal fatigue reliability [1]. Many of the Weibull plots also contain either early failures (Figures 7-10) or indications of multiple failure modes.

To enable a better understanding of the statistical results, basic failure mode analysis was performed on samples that failed during temperature cycling. Focus was placed on test cells with statistical or physical anomalies, such as low β or high incidence of early failures. Because test samples were not removed from the chamber immediately at the time of failure, identification of the first failure location was not always definitive. Unfortunately, retention samples were not included in the original test matrix, so there was no baseline (time zero) characterization for comparison to the failed, temperature cycled components.

Table 5. Summary of characteristic lifetimes (η) and slopes (β) for Pb free alloys tested in full and depopulated (perimeter) arrays. Metallographic failure mode analysis was performed on the shaded test cells

Pb free Alloy	Full Array		Depopulated (Perimeter) Array	
	η	β	η	β
SAC405	1019	3.0	1169	26.4
Sn3.5Ag	1196	9.2	1110	6.8
SAC310	952	2.4	678	4.1
SN100C	1108	2.7	439	5.6
SAC108	787	1.7	400	6.6
SAC105	1225	3.5	332	2.8
SACX	676	2.8	313	5.7
SAC205N	1079	4.7	269	7.1
LF35	831	1.8	215	3.5

Optical metallography (cross-sectional analysis) was the primary tool used to study the failure characteristics. The initial step was to identify if the failure occurred at the package or PCB side of the solder joint. Package side failure is most common for BGA solder fatigue failures. The next step was to confirm the failure mechanism. The expected failure mechanism in accelerated temperature cycling is thermal fatigue through the bulk solder. Although more detailed characterization of microstructural evolution and phase identification using scanning electron microscopy is desirable for alloy comparisons, it is beyond the scope of the current work.

Representative photomicrographs of failed samples for several alloys are shown in Figures 13-20. This physical failure data provides an overview of the types of failures observed in this experimental program. It does not encompass all alloys and is not intended to provide an exhaustive overview or a direct comparison of failure modes for the entire alloy set.

LF35

Figure 13 shows photomicrographs for failed samples of alloy LF35 for both full and depopulated array test vehicles. The LF35 alloy was analyzed because: 1) the LF35-F cell has an atypically low Weibull slope, with β=1.8, and 2) the LF35-D cell has an extremely low characteristic lifetime (η=215 cycles) as well as indications of several premature failures. These photomicrographs show that the fractures are not always the typical solder fatigue fractures at the package side of the solder joints. Some of the failures are mixed mode fractures consisting of solder fatigue, void-assisted fatigue and interfacial or near-interfacial fractures. Additional analyses that are too detailed to present here, reveal that the probable 1st fail sites occur at the PCB side, with minimal solder fatigue damage at the package side of those failed joints. The LF35 test results appear to be compromised by the mixed mode failures and multiple failure locations. This result is qualitatively consistent with the low Weibull slopes, particularly for the LF35-D (β=1.8) and might account for the low characteristic lifetime and early failures. There is however, no evidence that these mixed failure modes are a direct consequence of the LF35 alloy composition.

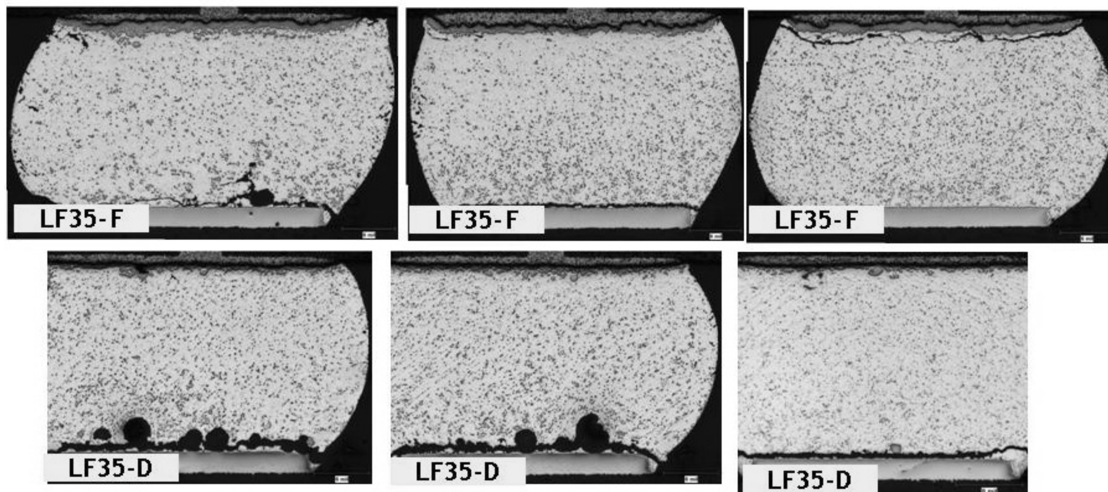

Figure 13. Photomicrographs for failed samples of alloy LF35 showing examples of solder fatigue, void-assisted solder fatigue and interfacial type fractures.

SAC310

Figure 14 shows photomicrographs of failed SAC310 alloy samples in both full and depopulated arrays. SAC310 was selected for analysis primarily because the SAC310-D cell has a characteristic lifetime, η=679 cycles, that is lower than expected compared to the other high Ag alloys such as SAC405 and Sn3.5Ag . The SAC310-F test cell also has a relatively low Weibull slope, with β=2.4. The analysis of the SAC310 fractures shows PCB side mixed mode failures with void-assisted fatigue and near-interfacial fractures. Figure 15 shows two examples of interfacial or near-interfacial fractures in SAC310 at higher magnification. These photomicrographs illustrate that it is very difficult to determine if the fracture path is through the solder adjacent to the intermetallic layer (near-interfacial) or between the solder and the intermetallic layer (interfacial).

Examination of multiple solder joints showed that the voiding was relatively severe in the case of 310-D and is likely responsible for low observed characteristic lifetime. Even though these photomicrographs are limited to a single sample, the data indicate that there is a strong possibility that the characteristic lifetime and slope are compromised by the presence of multiple and mixed mode failures. Qualitatively, the observed deviation from the pure fatigue failure mode seems greater for 310-D than 310-F.

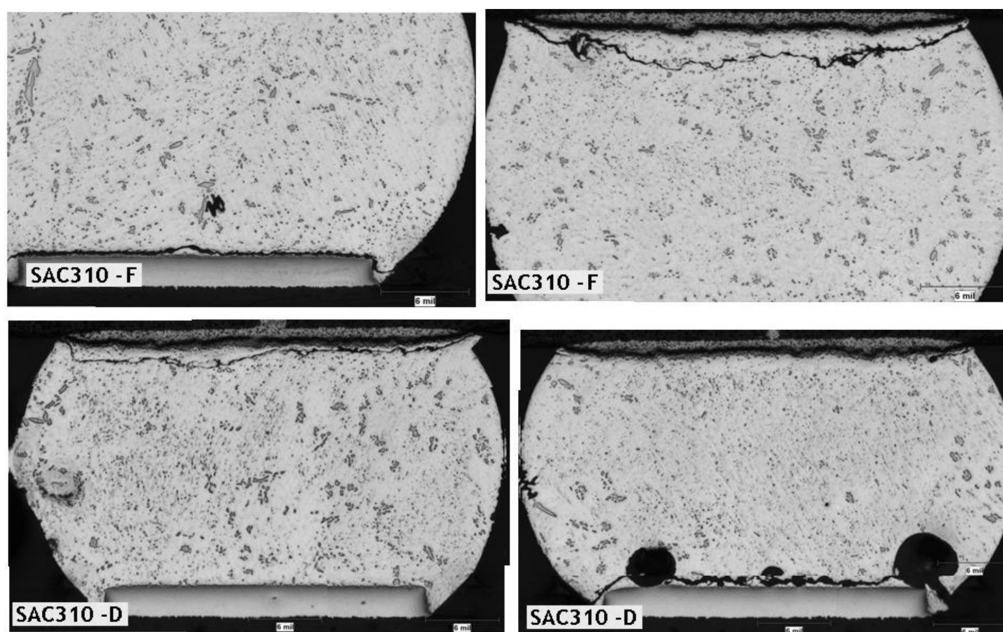

Figure 14. Photomicrographs for failed samples of alloy SAC310 showing examples of solder fatigue, void-assisted solder fatigue and interfacial type fractures.

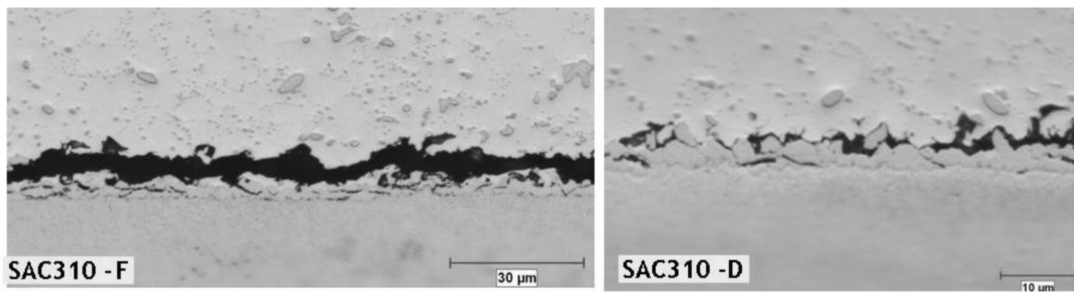

Figure 15. This figure shows higher magnification photomicrographs for interfacial or near-interfacial fractures in alloy SAC310.

SAC205+Ni (SAC205N)

Figure 16 shows photomicrographs for six failed BGA sites for alloy SAC205N in the full array configuration. SAC205N was chosen for analysis because of a relatively high characteristic lifetime (η=1079 cycles), and good β (4.7), which is indicative of a single failure mode such as solder fatigue. The SAC205N analysis shows that all the fractures in the outer rows of this particular component were due to solder fatigue at the package side. The Weibull plot for SAC205N (Figure 18) shows only two early, lower-cycle data points in the failure distribution (between 500 and 600 cycles), with the remainder of the failures above 900 cycles. These observations tend to support the conclusion that the SAC205N failure distribution is dominated by solder fatigue, with the possibility of a few early, mixed mode failures.

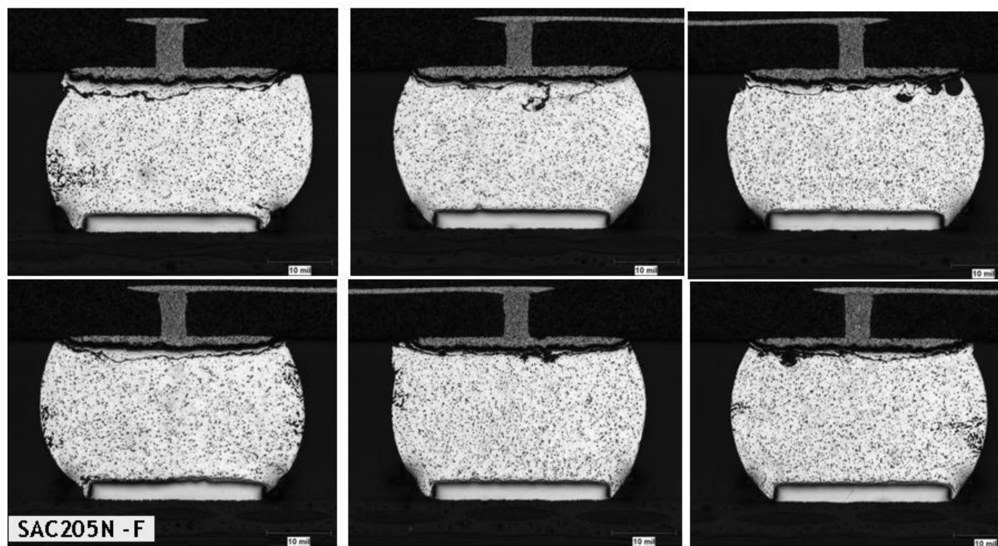

Figure 16. Photomicrographs for failed samples of alloy SAC205N showing only solder fatigue fractures.

SAC105 and SAC108

Based on a nominal Ag content of 1 wt.%, SAC alloys 105 and 108 are expected to have very similar thermal fatigue performance. Additionally, they are expected to have much lower fatigue resistance than the higher Ag alloys such as SAC405 and Sn3.5Ag. The data in Table 5 do not confirm these expectations. SAC105 has a substantially higher characteristic lifetime than SAC108 with the full array test vehicle, whereas SAC108 has a slightly higher characteristic lifetime in the test using the depopulated array. With the full array, SAC105 appears to have a characteristic lifetime comparable to both SAC405 and Sn3.5Ag.

The compositions of the original SAC105 and SAC108 solder balls prior to BGA attachment were determined quantitatively using atomic emission spectroscopy (AES). The results in Table 6 indicate that the original solder balls were within specification and there are no compositional anomalies, particularly with respect to the Ag content, which is believed to control thermal fatigue resistance. It can be concluded from this analysis that the perceived differences in alloy performance can not be attributed to deviations in the baseline compositions of the alloys.

Table 6. Analyzed composition of SAC105 and SAC108 solder balls prior to BGA ball attachment.

Pb free Alloy	Element (weight per cent)			
	Ag	Cu	Sn	other
SAC105	0.88	0.47	98.59	0.06
SAC108	0.98	0.78	98.14	0.10

A close examination of the Weibull plots for these alloys (Figures 8 and 10) shows some early failures as well as indications of multiple failure modes within the distributions. These data sets also are characterized by inconsistent Weibull slopes (β), which is indicative of some deviation from a single mode of fatigue failure. Failure analysis was performed on samples of SAC105 and SAC105 in an attempt to resolve these anomalies.

The series of photomicrographs in Figures 17-19 show clear evidence of the type of mixed mode solder joint fractures detected in the SAC310 and LF35 alloys. In general, the depopulated array samples seemed to have a greater tendency for anomalous failures than the full arrays, which is consistent with the results for the other alloys. This physical data, combined with the anomalies that exist in the Weibull plots, provide compelling evidence that the test data for SAC105 and 108 are compromised to a certain extent by non-fatigue type failure modes.

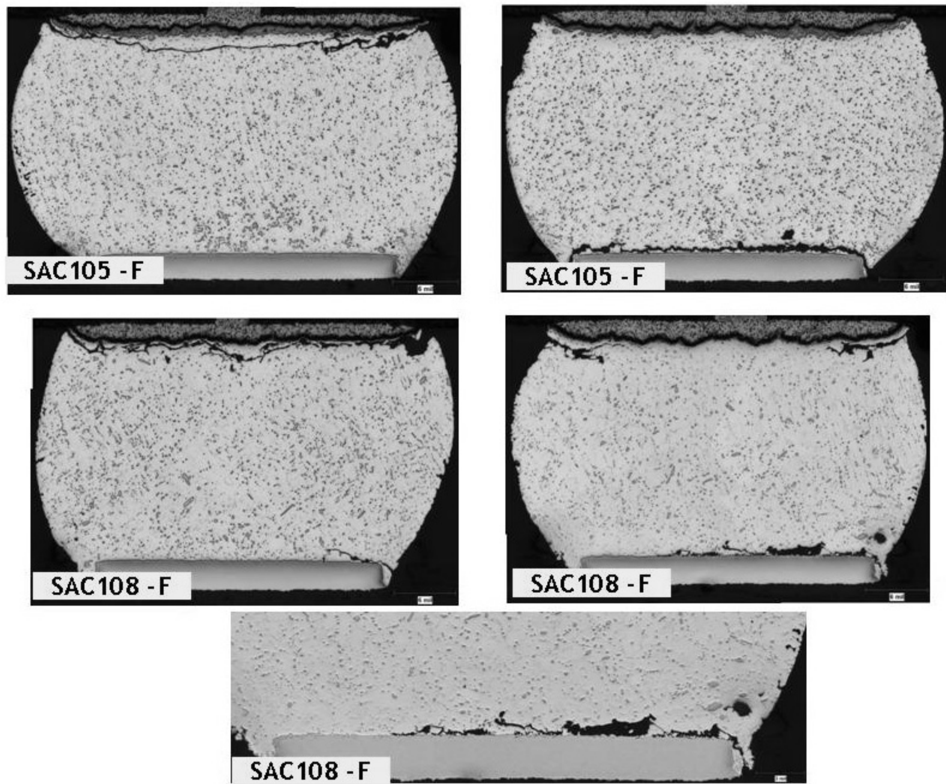

Figure 17. Photomicrographs showing both package and PCB side failures in SAC105 and SAC108 full array samples.

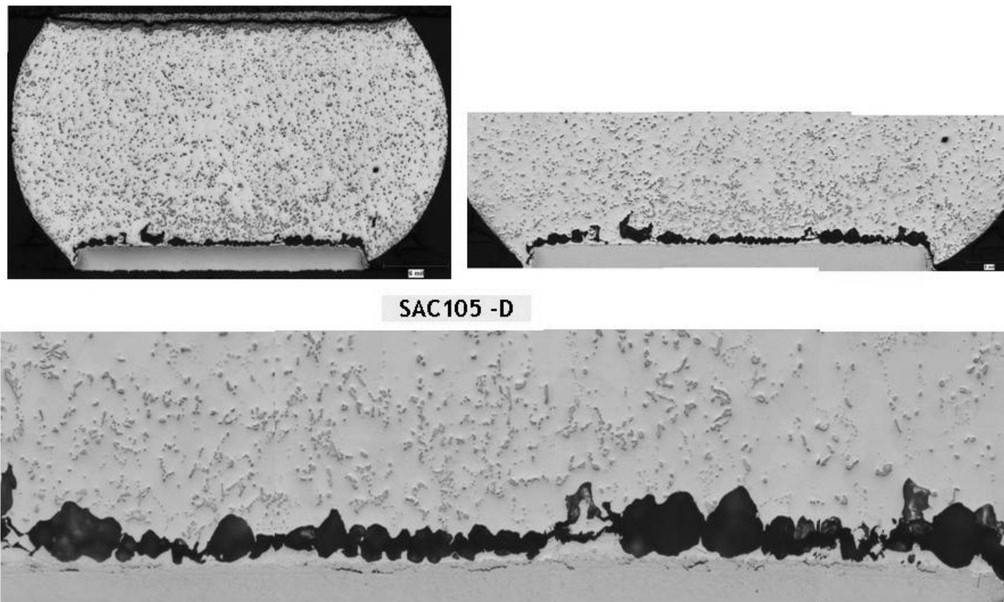

Figure 18. Photomicrographs showing void-assisted fracture in SAC105 in a depopulated array test sample.

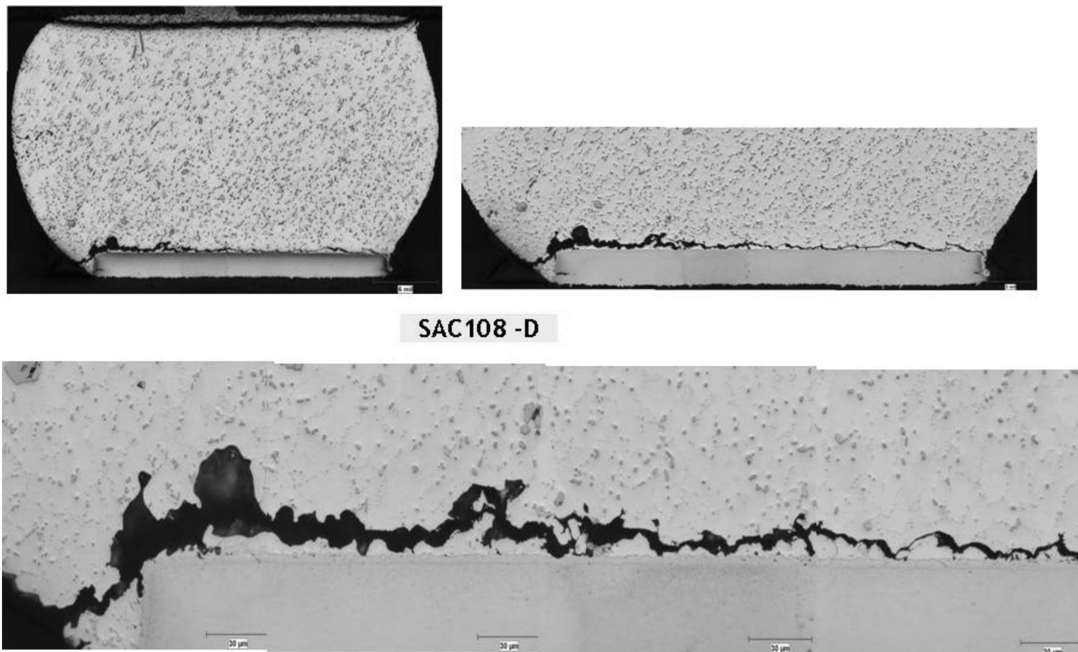

Figure 19. Photomicrographs showing multiple failure modes including void-assisted fracture and solder fatigue in a SAC108 depopulated array test sample.

SAC405 and Sn3.5Ag

The two highest-content Ag alloys, SAC405 and Sn3.5Ag, have consistently high characteristic lifetimes (η) with both the full and depopulated array test vehicles. The Sn3.5Ag has Weibull parameters characteristic of single mode, thermal fatigue failures. In the case of SAC405, the Weibull slopes (β) are not consistent, with the full array having a low β (3.0) and the depopulated array having an anomalously high β (26.4). The SAC405-F data exhibit an inexplicable bimodal distribution that is a major contributing factor to the low β value.

Unfortunately, the failure analyses on the SAC405 test vehicles did not resolve the anomalies or provide any further clarification of the test data. The photomicrographs of the SAC405-F and SAC405-D test vehicles in Figure 20 show that these two samples failed exclusively in solder fatigue at the package sides of the solder joints. Both the full and depopulated arrays selected for analysis failed at over 1000 cycles, which is completely consistent with the observed solder fatigue failure mechanism. It is conceivable that mixed mode failures could exist in some of the SAC405-F samples that failed at much

lower cycle counts. The presence of a few mixed mode failures in the distribution could lower the Weibull slope (β) without causing a significant drop in the characteristic lifetime. It would require substantial additional failure analysis in order to identify mixed mode failures, and that is beyond the scope of the current work. At this time, the authors are unable to offer an explanation for the extremely high β=26.4 for the SAC405-D.

The Sn3.5Ag-F sample also failed exclusively in solder fatigue at the package sides of the solder joints. It is interesting to note that some voiding is detected at the PCB side of the solder joint. The voiding in the Sn3.5Ag sample is not as severe compared to the other test cells and it is not a factor in the solder joint failure. However, this is further evidence of solder anomalies, even in a sample exhibiting acceptable performance in temperature cycling.

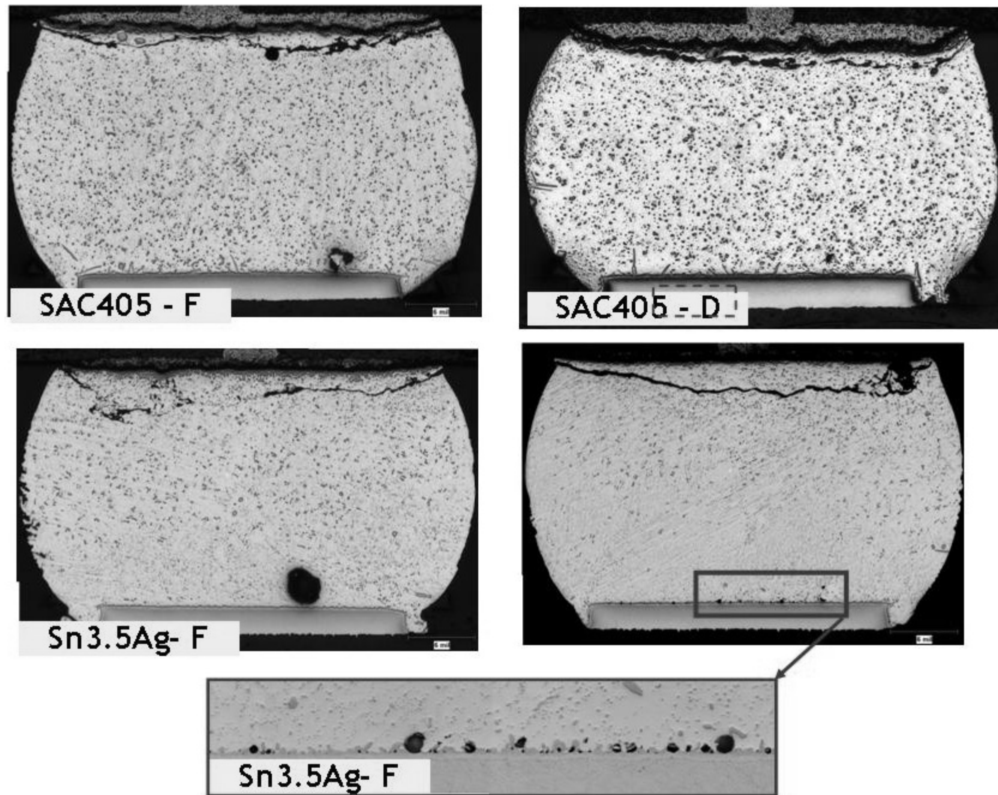

Figure 20. Photomicrographs for failed samples of alloy SAC405-F, SAC405- D and Sn3.5Ag-F showing only solder fatigue fractures at the package sides of the solder joints. There is voiding present at the PCB interface in the Sn3.5Ag but it there no cracking has initiated at that location.

Failure Analysis Summary

Metallographic failure analysis was performed on temperature cycled samples in order to obtain a better understanding of certain anomalies in the experimental Weibull data. Some of the anomalous Weibull statistical data can be explained at least qualitatively, in terms of the findings from the physical failure analysis.

In general, the following observations apply to results from the metallographic failure analysis:

- The first failures do not always occur by the expected thermal fatigue mechanism through the bulk solder. In addition to bulk solder fatigue, solder joint crack propagation also proceeds by void-assisted fatigue and interfacial or near-interfacial fracture.
- The first failures do not always occur as expected at the package side of the solder joint. The failures that occur at the PCB side typically result from mixed mode cracking.
- There is evidence that first failures characterized by mixed mode cracking at the PCB side, occur earlier in the distribution of failures.
- Because the presumed failure mode is thermal fatigue, these mixed mode failures tend to compromise the statistical analysis of the temperature cycling data.
- There is a higher incidence of mixed mode and PCB-side failures in the depopulated arrays.

The following observations apply to results for specific alloy test cells:

- The data for alloy LF35 is severely compromised by mixed mode failures. Void-assisted fatigue fracture located at the PCB side appears to be a major contributor to early failures in this test cell. Calculations of characteristic fatigue lifetime for LF35 are corrupted by the atypical failure modes.
- Mixed mode failures occur in SAC310, with the effect more pronounced in SAC310-D. The failure analysis indicates a strong possibility that both the characteristic lifetime and slope for SAC310-D are compromised by the presence of multiple and mixed mode failures. Mixed mode, early failures are likely responsible for the low slope in SAC310-F data and the low characteristic lifetime for SAC310-D.
- The analyses of the SAC205N and SAC405 samples show only fatigue cracking at the package side of the solder joints. The samples chosen for analysis failed at relatively high cycle counts in testing, which is consistent with fatigue failure. However, it must be noted that the Weibull plots for both of these alloys contain early failure data points or evidence of bimodal distributions, which is symptomatic of non-fatigue failures. The presence of mixed mode failures, particularly in SAC405-F could account for the low β in that test cell.
- The test results for SAC105 and 108 are compromised to a certain extent by non-fatigue type failure modes. The physical analysis and the anomalies in the Weibull plots, indicate that the apparent statistical distinction between the two alloys is an artifact introduced by atypical, non-fatigue failures.
- There is no correlation between alloy composition or specific alloying elements and the incidence of non-fatigue or mixed mode failures.

Detailed failure analysis was not performed on samples from every alloy test cell and additional work is needed to clarify some results from the current analysis. Nonetheless, every test cell that was examined was found to exhibit anomalous behavior in either the Weibull data or the physical failure analysis. Atypical non-fatigue mixed mode failures located at the PCB side of the solder joints could account for much of the anomalous behavior including: 1) rank order alloy variations between full and depopulated arrays, 2) atypically low Weibull slopes ($\beta<3.0$), 3) poor correlation between Ag content and reliability performance, and 4) early failures or indications of multiple failure modes in the Weibull

SUMMARY AND CONCLUSIONS

A thermal cycling study was conducted to obtain data comparing thermal fatigue reliability of the various Pb free solder ball alloys. The following conclusions can be drawn from the experimental results of this screening evaluation:

- Despite a number of anomalies in the experimental data, the thermal cycling data, Weibull analyses, and metallographic failure analysis indicate that the best thermal fatigue reliability performance was obtained with two alloys containing the highest Ag content. The SAC405 and binary eutectic Sn3.5Ag had a lower incidence of anomalies and consistently were the best performers with both the full and depopulated arrays.
- The SAC310 (the other high Ag alloy) data contained anomalies that produced a moderate reduction in the apparent characteristic lifetimes. However, this behavior could be explained largely by solder assembly quality defects detected in the failure analysis. Even with those data anomalies, SAC310 had performance in full and depopulated arrays, generally exceeding that of the lower Ag alloys.
- The SAC205N (Ni addition) performed nearly as well with the full array as the higher Ag alloys but the depopulated array performance was low.
- Based on previous results from the literature and direct comparisons with low Ag alloys in this work, the SN100C full array performed unexpectedly well. This is an inexplicable result and perhaps requires further study.
- The anomalies, particularly within the depopulated array data, preclude consistent, accurate rank ordering of the reliability performance of the alloys. With the exception of the three alloys with the highest Ag content, all other alloys had very low characteristic lifetimes when tested with the depopulated array.
- Atypical non-fatigue mixed mode failures located at the PCB side of the solder joints could account for much of the anomalous experimental observations including: 1) rank order alloy variations between full and depopulated arrays, 2) atypically low Weibull slopes ($\beta<3.0$), 3) poor correlation between Ag content and reliability performance, and 4) early failures or indications of multiple failure modes in the Weibull plots.
- There is no correlation between alloy composition or specific alloying elements and the incidence of non-fatigue or mixed mode failures.

RECOMMENDATIONS FOR ADDITIONAL WORK

The basic goal of the program was to conduct a limited sample size thermal cycling test that allowed screening the thermal fatigue performance of multiple Pb free solder alloys. That goal was accomplished but the presence of non-fatigue failure modes limited the ability to make comparisons such as detailed rank ordering. The results from the current screening process however, can be used to define additional thermal cycle testing, develop better data sets, and refine the alloy comparisons. The following recommendations are made for additional testing to enhance the current alloy comparisons:

- Use only the full array and increase the sample size per cell to 32.
- Limit the number of alloys tested by eliminating near-redundant compositions and certain low performing alloys. The following alloys are suggested for further, expanded study: SAC405 (or Sn3.5Ag), SAC310, SAC205N, and SN100C. This limited matrix provides a high Ag baseline control and includes those alloys that displayed promising thermal fatigue performance in the current screening study.
- Include time zero samples for baseline metallographic examination. This work should precede the thermal cycling to eliminate inclusion of assembly defects such as those discovered during failure analysis in the current screening study.
- Use the same temperature cycling parameters and if possible, the same thermal chamber used in the screening study.

ACKNOWLEDGMENTS

This work was done under the auspices of the HDP User Group International, Inc. The authors want to thank Marshall Andrews, HDP Executive Director, Laurence Schultz, Project Coordinator, and the HDP Board of Directors for their continued support of the project. The authors also want to recognize the support of the management teams from Alcatel-Lucent, Freescale Semiconductor, Sun Microsystems, Philips Medical, and Flextronics for additional resource support beyond the typical scope of project participation.

REFERENCES

[1] G. Henshall et al., "iNEMI Lead-Free Alloy Alternatives Project Report: Thermal Fatigue Experiments and Alloy Test Requirements" Proceedings SMTAI, 2009

[2] G. A. Henshall, et al., "iNEMI Pb-Free Alloy Alternatives Project Reports: State of the Industry," proceedings SMTAI, p. 109, 2008.

[3] G. A. Henshall, et al., "Addressing Industry Knowledge Gaps Regarding New Pb-Free Solder Alloy Alternatives," proceedings IEMT, p. B4.2, 2008.

[4] G. A. Henshall, et al., "iNEMI Pb-Free Alloy Alternatives Project Reports: State of the Industry," Journal of Surface Mount Technology, vol. 21, no. 4, p. 11, 2008

[5] G. A. Henshall, et al., "Addressing Opportunities and Risks of Pb-Free Solder Alloy Alternatives," proceedings EMPC, 2009.

[6] K Sweatman, S. Suenaga and T. Nishimura, "Strength of Lead-free BGA Spheres in High Speed Loading", Proceedings Pan Pacific, 2008.

[7] Ranjit S Pandher, Brian G Lewis, Raghasudha Vangaveti and Bawa Singh, "Drop Shock Reliability of Lead-Free Alloys – Effect of Micro-Additives," Proceedings 57th Electronic Components and Packaging Technology (ECTC), Reno, May 29-June 1, 2007.

[8] Ranjit S Pandher, Robert Healey, "Reliability of Pb-Free Solder Alloys in Demanding BGA and CSP Applications," Proceedings 58th Electronic Components and Packaging Technology (ECTC), Orlando, May 27-30, 2008.

[9] H. Kim, et al., "Improved Drop Reliability Performance with Lead Free Solders of Low Ag Content and Their Failure Modes," Proceedings ECTC, p. 962, 2007.

[10] A. Syed, et al., "Effect of Pb free Alloy Composition on Drop/Impact Reliability of 0.4, 0.5 & 0.8mm Pitch Chip Scale Packages with NiAu Pad Finish," Proceedings ECTC p. 951, 2007.

[11] D. Kim, et al., "Evaluation of High Compliant Low Ag Solder Alloys on OSP as a Drop Solution for the 2nd Level Pb-Free Interconnection," Proceedings ECTC p. 1614, 2007.

[12] A. Syed, T. Kim, S Cha, "Alternate Solder Balls for Improving Drop/Shock Reliability," Proceedings SMTAI, p. 390, 2007.

[13] S.K. Kang et al., "Evaluation of Thermal Fatigue Life and Failure Mechanisms of Sn-Ag-Cu Solder Joints with Reduced Ag Contents," Proceedings ECTC 2004.

[14] S. Terashima et al., “Effect of Silver Content on Thermal Fatigue Life of Sn-xAg-0.5Cu Flip-Chip Interconnects,” J. Electronic Materials, Vol. 32, no. 12, 2003

[15] G. Henshall et al., “Comparison of Thermal Fatigue Performance of SAC105 (Sn-1.0Ag-0.5Cu), Sn-3.5Ag, and SAC305 (Sn-3.0Ag-0.5Cu) BGA Components with SAC305 Solder Paste,” Proceedings APEX, p. S05-03, 2009.

[16] Richard Coyle, et al., “The Influence of the Pb free Solder Alloy Composition and Processing Parameters on Thermal Fatigue Performance of a Ceramic Chip Resistor, Proceedings 59th ECTC, 423-430, May 26-29, 2009.

[17] Ranjit S Pandher, Robert Healey, “Reliability of Pb-Free Solder Alloys in Demanding BGA and CSP Applications,” Proceedings 58th Electronic Components and Packaging Technology (ECTC), Orlando, May 27-30, 2008.

[18] J. Pan, “Lead-Free Liquidus Temperature Calculator,” http://www.calpoly.edu/~pan/LTCalculator.html (2008).

[19] IPC-9701A, “Performance Test Methods and Qualification Requirements for Surface Mount Solder Attachments,” IPC, Bannockburn, IL, (2006).

Appendix A
Individual Weibull Plots by Alloy

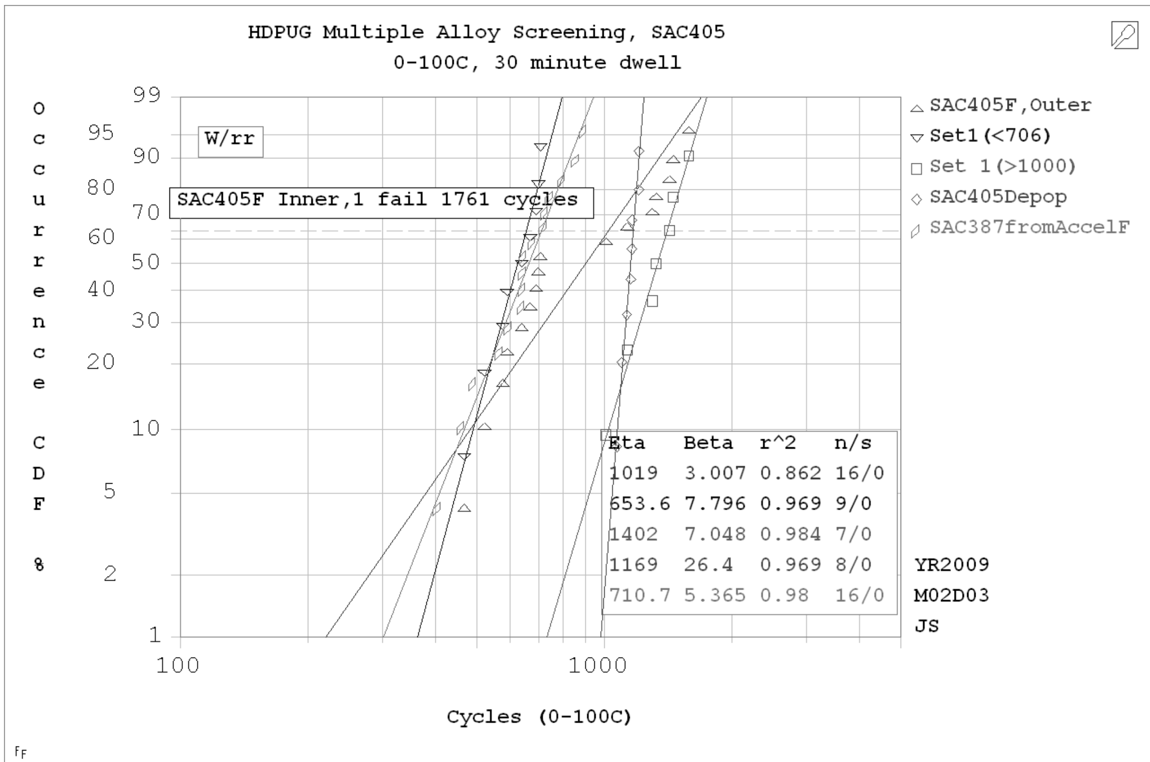

Figure A1: SAC405 Weibull plots including the comparable Weibull plot on the same component used in the HDPUG acceleration factors test.

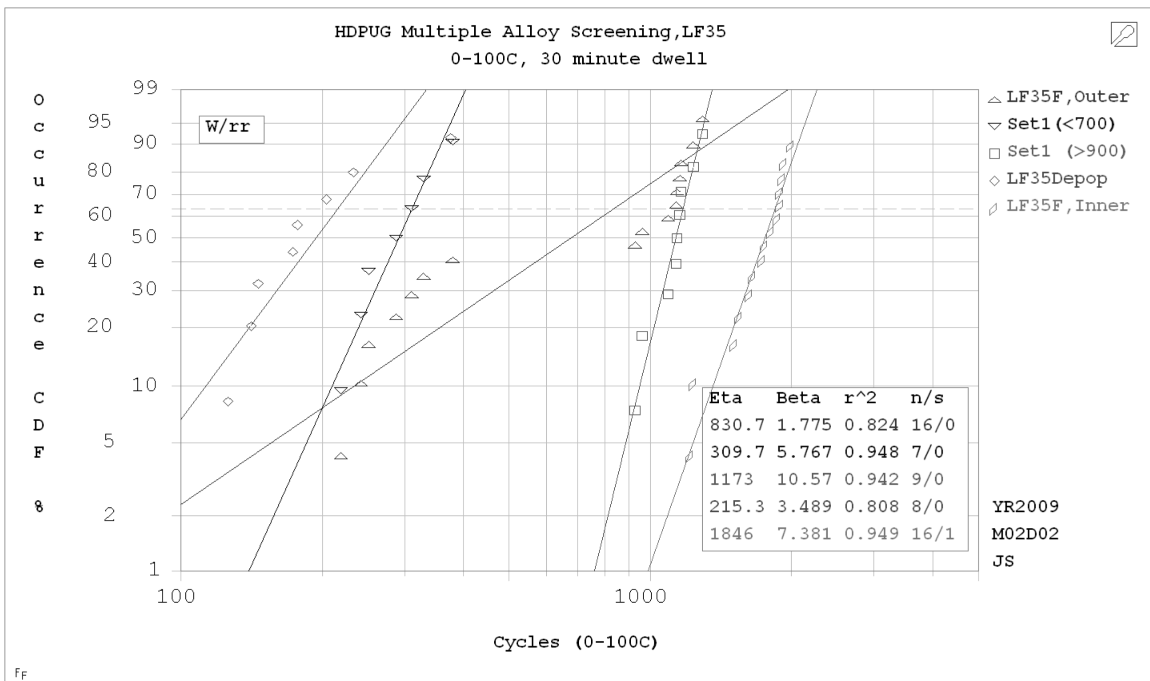

Figure A2: LF35 Weibull plots

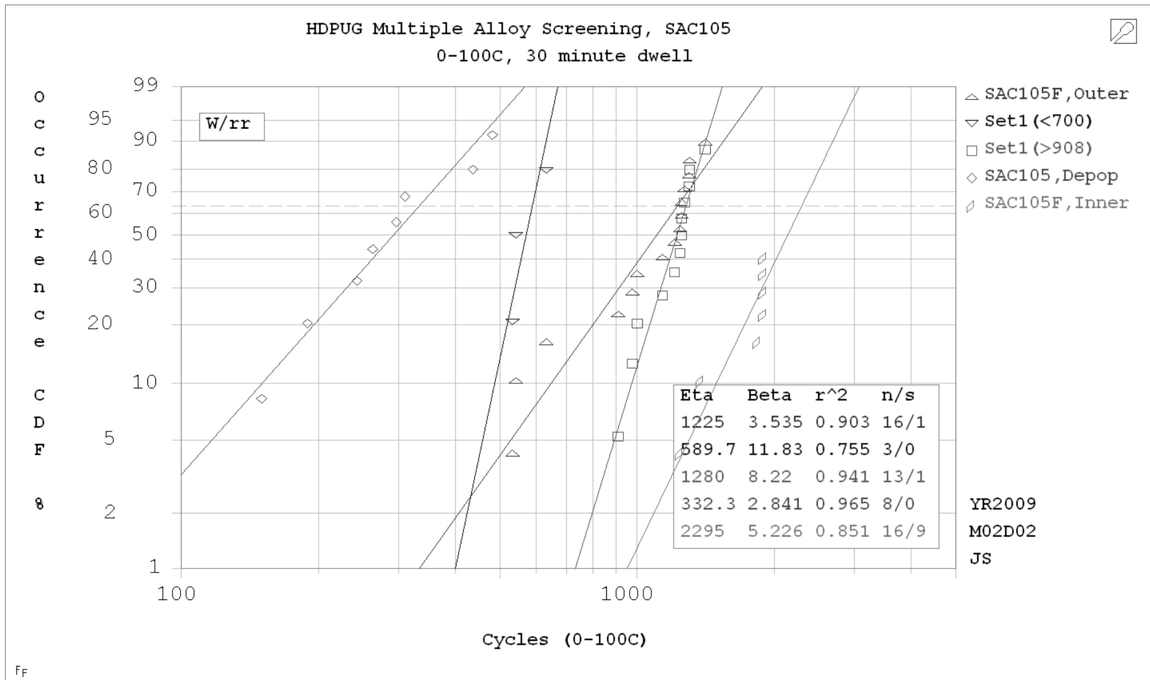

Figure A3: SAC 105 Weibull plots

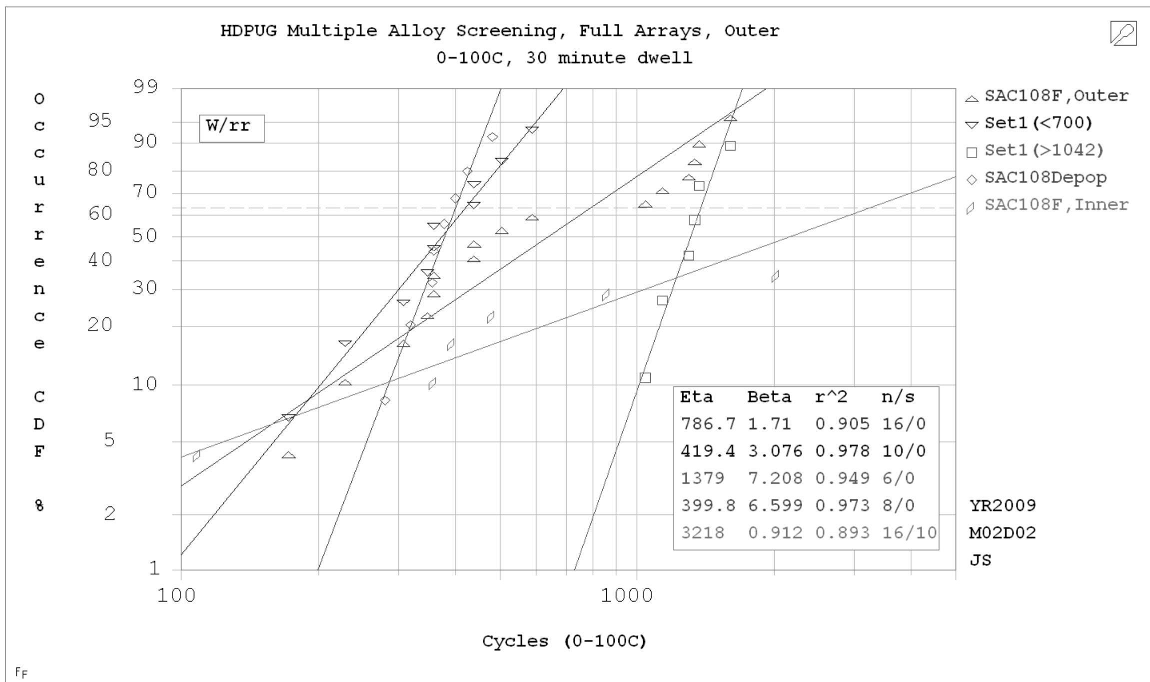

Figure A4: SAC108 Weibull plots

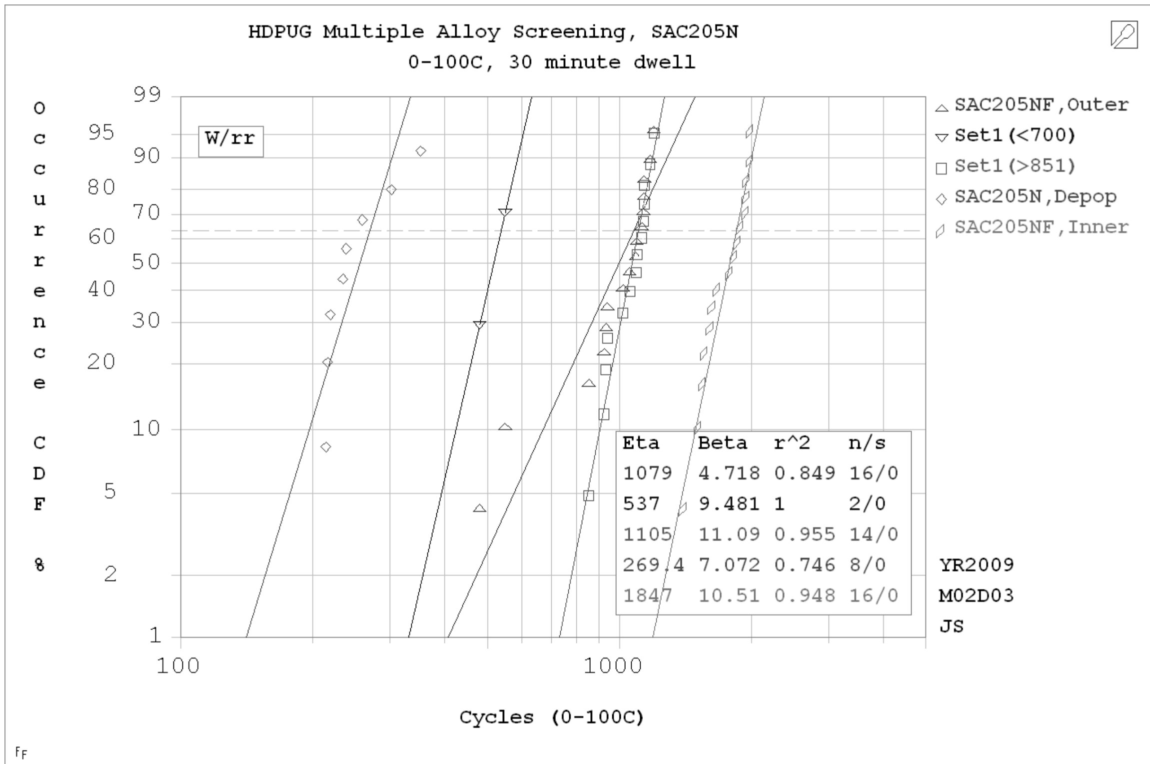

Figure A5: SAC205N Weibull plots

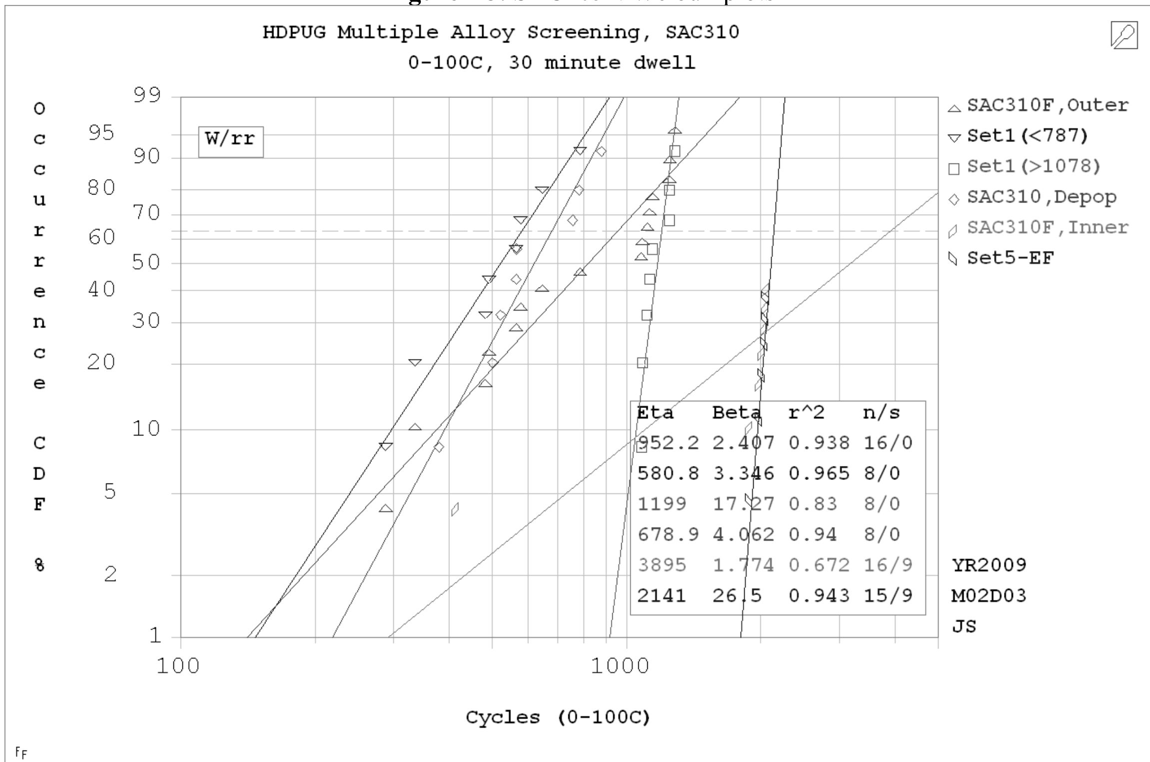

Figure A6: SAC 310 Weibull plots

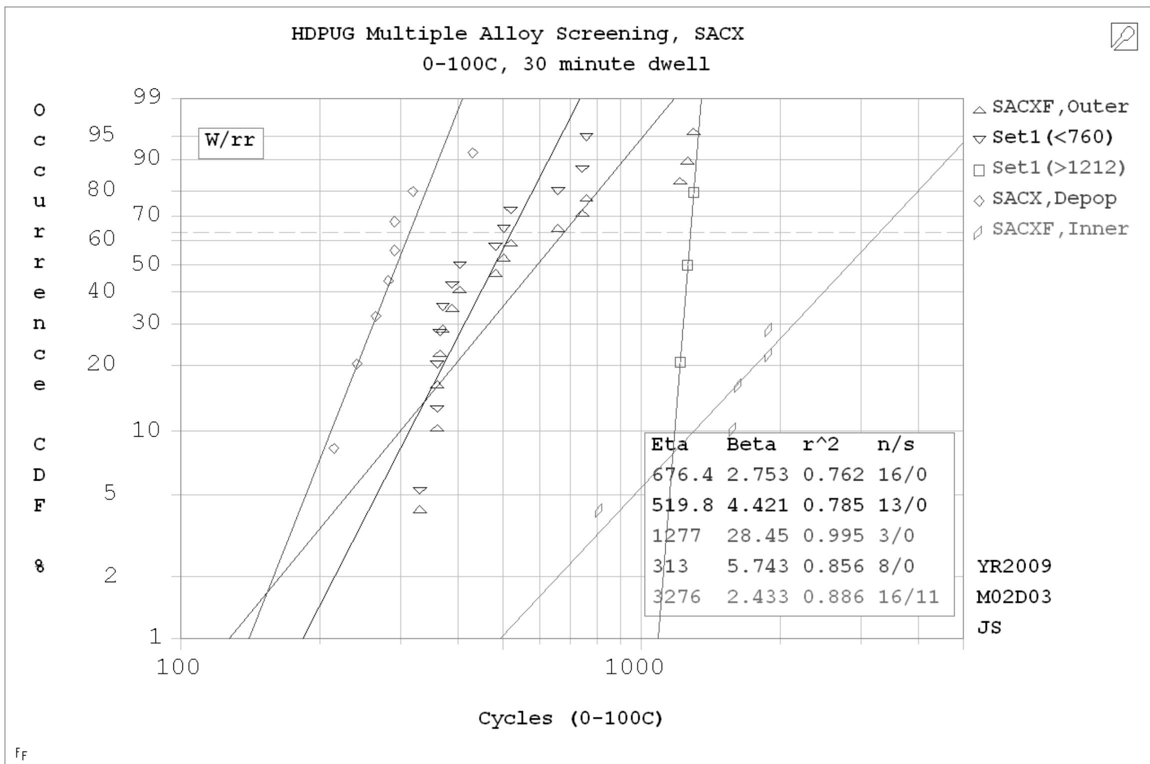

Figure A7: SACX Weibull Plots

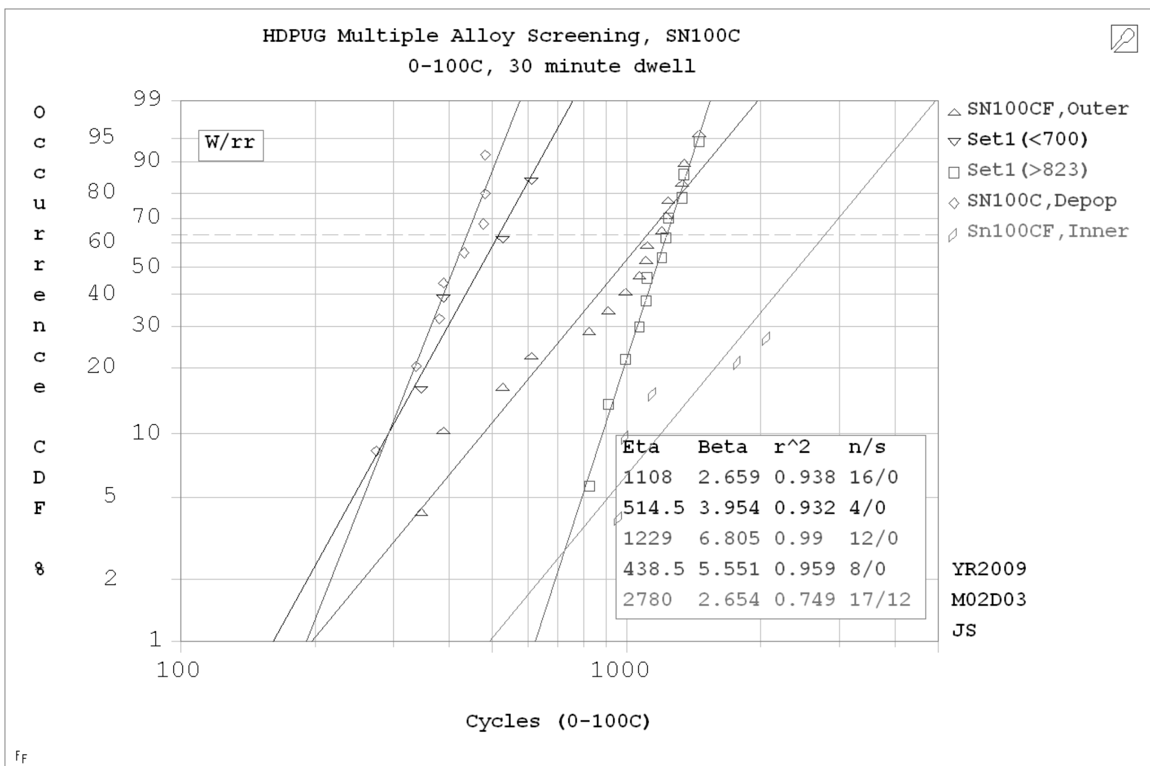

Figure A8: SN100C Weibull Plots

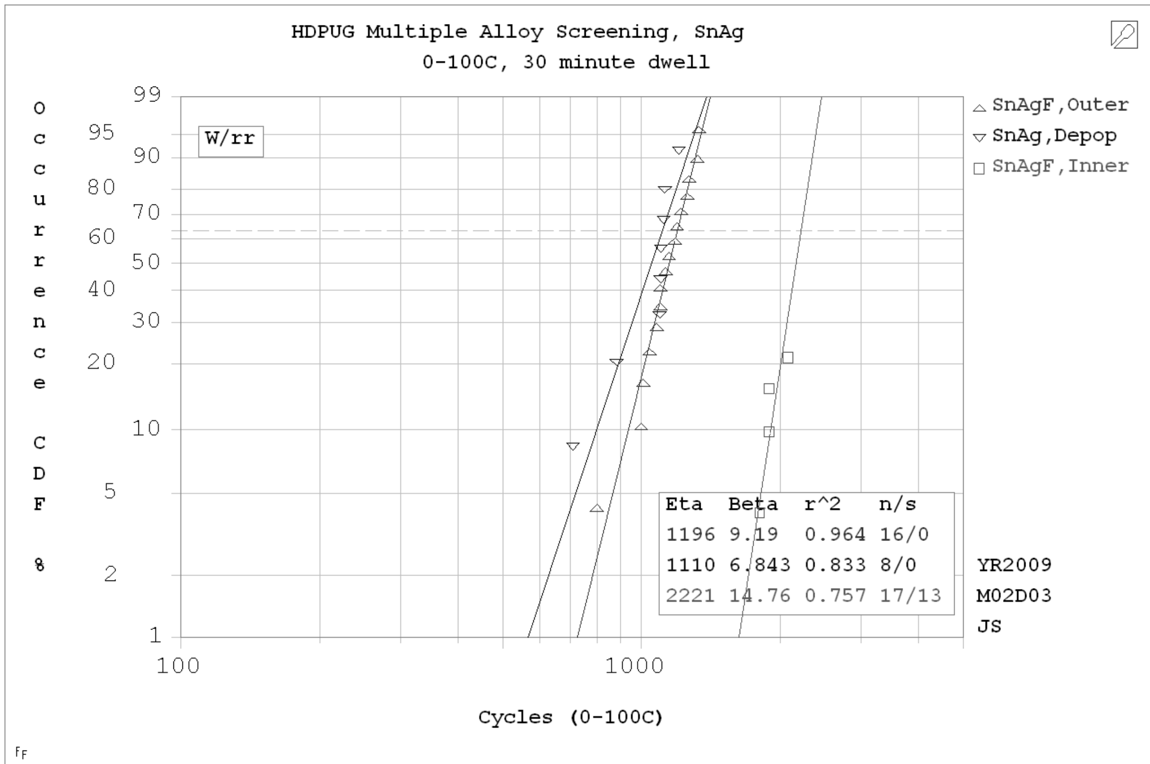

Figure A9: SnAg Weibull Plots